Tilting-Pad Journal Bearings with Active Lubrication Applied as Calibrated Shakers: Theory and Experiment

Cerda Varela, Alejandro Javier; Santos, Ilmar

Published in:
Journal of Vibration and Acoustics

Link to article, DOI:
10.1115/1.4028452

Publication date:
2014

Document Version
Peer reviewed version

Tilting-Pad Journal Bearings with Active Lubrication Applied as Calibrated Shakers: Theory and Experiment

Alejandro Cerda Varela*
Department of Mechanical Engineering
Technical University of Denmark
2800 Kgs. Lyngby, Denmark
Email: acer@mek.dtu.dk

Ilmar Ferreira Santos
Department of Mechanical Engineering
Technical University of Denmark
2800 Kgs. Lyngby, Denmark
Email: ifs@mek.dtu.dk

ABSTRACT

In recent years, a continuous research effort has transformed the conventional tilting-pad journal bearing into a mechatronic machine element. The addition of electromechanical elements provides the possibility of generating controllable forces over the rotor as a function of a suitable control signal. Such forces can be applied in order to perform parameter identification procedures in-situ, which enables evaluation of the mechanical condition of the machine in a non-invasive way. The usage of a controllable bearing as a calibrated shaker requires obtaining the bearing specific frequency dependent calibration function, i.e. the transfer function between control signal and force over the rotor. This work presents a theoretical model of the calibration function for a tilting-pad journal bearing with active lubrication. The bearing generates controllable forces by injecting pressurized oil directly into the bearing clearance. The injected flow is controlled by means of a servovalve. The theoretical model includes the dynamics of the hydraulic system using a lumped parameter approach, which is coupled with the bearing oil film using a modified form of the Reynolds equation. The oil film model is formulated considering an elastothermohydrodynamic lubrication regime. New contributions to the mathematical modeling are presented, such as the inclusion

*Address all correspondence to this author.

of the dynamics of the hydraulic pipelines, and the obtention of the bearing calibration function by means of harmonic analysis of a linearized form of the controllable bearing constitutive equations. The mathematical model is used to study the relevance and effects of different parameters on the calibration function, aiming at providing general guidelines for the active bearing design. Finally, experimental results regarding the calibration function and the usage of the studied bearing as a calibrated shaker provide insight into the possibilities of application of this technology.

Nomenclature

ALB Actively lubricated bearing

A_P Pipeline cross section area

$\mathbf{A}$ System matrix for Reynolds equation discretized solution

$\mathbf{b}$ Pad modal coordinates vector

β Equivalent bulk modulus oil flow

$C(\omega)$ Bearing calibration function, frequency domain

$c_0 = \sqrt{\frac{\beta}{\rho}}$ Speed of sound

c_P Pipeline linearized damping coefficient

$\mathbf{D}_{ALB}$ Linearized global damping matrix

d_{inj} Pad injection nozzle diameter

δi Linearized i-variable

ξ_V Servovalve damping ratio

$F_{active}(\omega)$ Bearing active forces, frequency domain

F_{ext} Pipeline oil flow external forces

$FRF(\omega)$ Frequency response function

$\mathbf{f}_{ext}$ External force over the journal

$\mathbf{f}_r$ Pressure field resultant force over the journal

$\mathbf{f}_b$ Pressure field resultant force over the bearing pad

$g(\hat{x},\hat{z})$ Pad orifice shape function

γ_{P_i} Pipeline i-th acoustic modal flow

H_i Pipeline i-th acoustic normal mode

$h(\hat{x},\hat{z})$ Oil film thickness

K_{pq} Servovalve flow pressure coefficient

$\mathbf{K}_b$ Bearing pad stiffness matrix

$\mathbf{K}_{ALB}$ Linearized global stiffness matrix

L_P Pipeline length

l_{inj} Pad injection nozzle length

$\mathbf{M}_r$ Journal mass matrix

$\mathbf{M}_b$ Bearing pad mass matrix

$\mathbf{M}_{ALB}$ Linearized global mass matrix

μ Oil viscosity

p_P Pressure pipeline, time domain

$p(\hat{x},\hat{z},t)$ Oil film pressure field

p_{inj} Pressure injection nozzle

$\mathbf{p}$ Discretized oil film pressure field

$\mathbf{p}_{inj}$ Injection pressure vector

q_V Servovalve flow

q_V^* Servovalve leakage flow

q_{x_V} Servovalve spool driven flow, time domain

q_P Flow pipeline, time domain

$\mathbf{q}_P$ Injection flow vector

R Journal Radius

R_V Servovalve flow voltage coefficient

r_P Pipeline cross section radius

ρ Oil density

S_q Pipeline sources/sinks

$\mathbf{s}$ Global system state vector

$\mathbf{s}^*$ Global system state vector in static equilibrium

$U(\omega)$ Servovalve control signal, frequency domain

u_V Servovalve control signal, time domain

$v_{inj}(\hat{x},\hat{z},t)$ Injection flow velocity profile

$\mathbf{V}$ Pad modal matrix

$\mathbf{W},\mathbf{Q}$ System matrix for Reynolds equation solution, Hagen-Pouiseuille injection flow

$\hat{x},\hat{y},\hat{z}$ Oil film curvilinear reference frame

x_V Servovalve spool position, time domain

x_P Pipeline longitudinal position

$\mathbf{x}_r$ Journal center position vector

$Y(\omega)$ Journal vertical displacement, frequency domain

Ω Journal rotational speed

ω_V Servovalve cut-off frequency

ω Frequency

ω_{P_i} Pipeline i-th acoustic natural frequency

1 Introduction

The challenges related to the design and operation of turbomachinery for industrial applications, such as energy extraction and conversion, are steadily increasing. Current trends demand for increased efficiency, availability and adaptability of these machines. In this context, bearing design is of the uttermost importance, since it is crucial to determine the dynamic behavior of the machine as a whole.

Tilting-pad journal bearings (TPJB) are commonly used in turbomachinery, due to its improved stability characteristics when compared to other fluid film bearings alternatives [1, 2]. Although a versatile design, its static, thermal and dynamic properties are "fixed" at the design stage. Consequently, its traditional configuration does not give room for adapting to different operational scenarios. The need for including these characteristics into the TPJB design opened a new research front, aimed at transforming it into a mechatronic machine element, through the combination of mechanical and electronic components.

Over time, a number of authors have worked theoretically and experimentally with this objective in mind, following different strategies. The first ideas were presented by Ulbrich and Althaus in 1989 [3]. They theoretically analyzed the usage of piezoelectric actuators to adjust the bearing clearance, in order to control the bearing characteristics. Another approach was implemented theoretically and experimentally by Santos [4,5], considering the installation of hydraulic chambers in the back of the pads and a servovalve to dynamically regulate the pressure within the chambers. Regarding the design of controllers for mechatronic tilting-pad bearings, some theoretical studies have been carried out by Deckler *et al.* [6] and Wu and De Queiroz [7], considering the usage of linear actuators in the back of the pad and also rotational actuators, acting directly over the tilting angle of the pad. Wu and De Queiroz investigated some of their ideas experimentally, by building and testing a tilting-pad bearing design featuring controllable pushers in the back of the pads [8].

A different strategy to achieve a mechatronic TPJB design was firstly introduced in 1994 by Santos [4]. The actively lubricated bearing (ALB) design features a modified pad geometry, that includes a nozzle located across the pad in the radial direction. Pressurized oil is injected directly into the bearing clearance through these nozzles. The injected oil flow can be modified by means of a servovalve, which is controlled by an electric signal generated in a processing unit. As a result, the oil film pressure field is altered, with the resulting modification of the bearing properties.

The validity of the ALB concept has been proven experimentally in a number of studies. The modification of the static and thermal properties of the TPJB as a result of the oil injection was shown in [9]. Its ability to modify the TPJB dynamic coefficients was studied in [10]. In [11], it was applied as the actuator of a control loop, aimed at controlling the vibrations of a rigid rotor setup. Similar results, but concerning the control of vibrations of a flexible rotor, were presented in [12].

The ALB is capable of generating controllable forces over the rotor, as a function of an input signal. This concept was tested experimentally in [12, 13], proving that it is possible to generate forces in a wide frequency range. This feature provides the possibility of using it as a calibrated shaker for performing parameter identification in turbomachinery. Since the ALB can be included as a permanent component of the machine, such test can be performed in a non invasive way, without the need of mounting external actuators or sensors. By obtaining modal parameters in situ, it could be possible to validate the mathematical simulation tools available for the machine, or to detect faulty conditions.

This field of application demands for a characterization of the ALB calibration function, meaning the relationship between

input signal and active force over the rotor. Since a parameter identification procedure is usually performed in frequency domain, the calibration function must be obtained as a function of the input signal frequency. In [13], the calibrated forces generated by the ALB were determined using a purely experimental approach, as a function of frequency and Sommerfeld number (i.e. bearing static load and journal rotational speed). Although the results arising from this method were satisfactory, it is also desirable to be able to predict this calibration function by theoretical means, in order to study the effect of different design parameters over the ALB calibrated forces. This approach requires a mathematical model that represents in a reduced manner the interaction between the physical domains existing within the ALB, i.e. hydraulics, oil film and bearing pad dynamics.

The current theoretical model for the ALB corresponds to an elastothermohydrodynamic formulation, that includes the oil injection effect in a simplified way [14–17]. In this article, this model is used as the framework for developing a method to obtain the ALB calibration function by theoretical means. The main original contributions correspond to the inclusion of pipeline dynamics effects into the theoretical model, and the obtainment of the calibration function by means of harmonic analysis of a linearized version of the ALB governing equations. Furthermore, experimental results regarding the ALB calibration function and the usage of the studied bearing as a calibrated shaker provide insight into the possibilities of application of this technology.

2 Experimental Setup

2.1 The ALB Test Rig

The ALB test rig at the Technical University of Denmark (DTU) has already been extensively used in [9, 13, 18] to investigate the static and dynamic behavior of this specific controllable bearing design. The reader should refer to the cited references for a complete presentation of the experimental setup.

The setup consists of a test bearing, a rigid rotor mounted in a tilting frame, and a hydraulic system, see Fig. 1. The driving unit is composed of an electric motor and a belt transmission. The parameters for the test rig are stated in Table 1. The tilting frame is pivoted in one end, allowing for vertical displacements of the rigid rotor attached to it, but fixing it in the horizontal direction. It also constrains the pitching movement of the rotor. Hence, the rotor position can be described using a single degree of freedom. The test bearing consists of two tilting pads located above and below the rotor, supporting it in the vertical direction. The most important component within the tilting pads design are the nozzles, see Fig. 2, aimed at injecting pressurized oil into the bearing clearance. The pressurized oil flow towards the injection nozzle is controlled by means of a single servovalve. Each of the two servovalve ports is connected to a nozzle via a steel pipe. By feeding an appropiate input signal into the servovalve, the oil flow towards each injection nozzle is altered, modifying the oil film pressure field. This entails a modification of the resultant forces over the rotor, rendering the bearing controllable.

2.2 Configurations

Two different configurations are used for obtaining the experimental results included in this study, as shown in Fig. 3. In both cases, the input signal fed into the servovalve corresponds to a chirp signal of known amplitude. Consequently, it is

possible to study the system behavior in a certain frequency range.

The first configuration enables one to determine experimentally the active forces over the rotor generated by the ALB. It considers fixing the tilting frame in a certain position, by means of an adjustment bolt located at the frame free end. This system enables to fix the vertical rotor position to a certain eccentricity. A load cell is associated with the adjustment bolt, and its measured force can be directly related to the resulting forces over the rotor, if no relevant dynamics from the tilting frame take place within the analyzed frequency range, i.e. the tilting frame behaves as a rigid body.

The second configuration enables one to obtain the frequency response function of the system when no restriction to its movement is applied, i.e. the adjustment bolt is not present. The displacement of the tilting frame free end is measured via a displacement probe, and can be directly related to the rotor vertical displacement. The system is excited using the forces generated by an electromagnetic shaker, or by the ALB injection system. This setup enables to study the feasibility of using the ALB for obtaining the system frequency response function, by using the results given by the electromagnetic shaker as benchmark.

3 Mathematical Modeling

The ALB calibration function $C(\omega)$ is the relationship between the servovalve input signal $U(\omega)$ and the resultant force over the rotor $F_{active}(\omega)$, as a function of the input signal frequency ω. It can be stated as:

$$C(\omega) = \frac{F_{active}(\omega)}{U(\omega)} \tag{1}$$

In general, $C(\omega)$, $U(\omega)$, $F(\omega)$ are complex magnitudes. This function can be obtained through purely experimental means, using the available experimental setup, as it was reported in [13]. However, it is relevant to obtain a mathematical model that enables accurate prediction of the ALB calibration function for a given set of design parameters.

The mathematical model for the ALB has been presented in a number of publications [14–17]. Its current formulation corresponds to an elastothermohydrodynamic lubrication regime, that includes the effect of the hydraulic system and oil injection in a simplified manner. For the sake of briefness, the model shall not be presented in full detail here, and the reader should refer to the cited literature for a complete presentation. In short, its main features are:

1. The oil film pressure field is modeled using a modified version of the Reynolds equation for incompressible laminar flow. It includes an extra term related to the oil injection that renders the bearing controllable. Further details can be found in [4, 14], and in the following sections of this paper.
2. The thermal model considers both the oil film and the pads as domains for the analysis, due to the heat transfer process taking place between them. The oil film energy equation and Fourier law for pad heat conduction are consequently solved in a coupled manner. The effect of the oil injection is included in the oil film energy equation considering convection and diffusion effects. Further information is available in [15, 17, 19, 20].

3. The pad and pivot flexibility are included using a pseudo modal reduction scheme, as initially proposed in [21]. The displacements of the pad solid domain are modeled as a linear combination of predefined mode shapes, associated with modal coordinates. The mode shapes represent the pad rigid body motions and elastic deformations. For further details, please refer to [16, 21, 22].
4. The numerical solution of the partial differential equations for oil film pressure field, thermal model and pad flexibility model is obtained using the finite element method. The weak form is obtained using the Bubnov-Galerkin method, except for the oil film energy equation, where a streamlined upwind Petrov-Galerkin formulation is implemented. Further details can be found in [23, 24].

Based on the previous research effort, this article expands the mathematical model and introduces two original contributions:

1. Inclusion of the dynamics related to the pipelines connecting the servovalve ports with the injection nozzles, in order to assess their effect on the ALB calibration function.
2. Calculation of the frequency dependent ALB calibration function, by means of harmonic analysis of a linearized form of the ALB governing equations.

For the sake of clarity, the mathematical presentation given here represents the ALB test rig presented previously (two pads, rotor with one degree of freedom, one servovalve and two pipelines). However, the procedure is general enough to be expanded to an ALB with a "free" rotor configuration, and different number of pads and servovalves. For any given case, the system contains one servovalve for each pair of pads. The presentation is focused on detailing the mathematical representation of the hydraulic system, the approach followed to couple it with the oil film pressure field model, and the linearization procedure of the resulting non linear system of equations.

3.1 Modeling the Hydraulic System: the Servovalve

For modeling the ALB, it is necessary to describe the pressurized oil flow reaching the injection nozzle in each one of the tilting pads, as a function of the control signal $u_V = Ue^{i\omega t}$. The flow is controlled by means of a servovalve, modeled following the approach stated in [4, 14].

The servovalve flow q_V can be linearized around an operational point defined by the centered position of its spool $x_V^* = 0$. Considering that the flow is a function of the spool position x_V and the load pressure p_L, a first order Taylor expansion yields [25]:

$$q_V = q_V^* + q_{x_V} + K_{pq} p_L \, , for \, x_V^* = 0 \tag{2}$$

In Eqn. (2) three terms can be distinguished: the leakage flow q_V^* observed when the spool is centered, the flow dependent on the spool position q_{x_V}, and the flow dependent on the load pressure $K_{pq} p_L$, linearized using the coefficient K_{pq}.

The spool position is controlled via the servovalve control signal u_V, yielding a modification of the spool position dependent flow q_{xV}. This relationship can be modeled [26–28] using a second order ordinary differential equation:

$$\ddot{q}_{xV} + 2\xi_V \omega_V \dot{q}_{xV} + \omega_V^2 q_{xV} = \omega_V^2 R_V u_V \tag{3}$$

The coefficients ξ_V,ω_V and R_V introduced in Eqn. (3) are properties of each servovalve, and they characterize the frequency dependency of the resulting servovalve flow q_V with respect to the input signal u_V.

3.2 Modeling the Hydraulic System: The Pipelines

The relevance of including the pipeline dynamic effects for modeling the behavior of hydraulic systems is well understood, hence a significant amount of literature is available on the subject [29–32]. For applications where a constant flow is imposed, the pipeline has relevant effects considering the system head losses. However, for cases where the input flow is modified harmonically with high frequencies, such as in the ALB hydraulic system, the dynamic effects related to their acoustic modes can significantly modify the resulting output flow. Therefore, the pipeline dynamics can have a significant effect on the ALB calibration function.

As with any other dynamic system, the inclusion of the pipeline dynamics into the mathematical model depends on the presence of resonance areas (in this case, acoustic resonances) in the frequency range of interest. The pipeline design parameters and the characteristics of the fluid, specially the amount of entrained air, can significantly reduce the acoustic natural frequencies [25, 33], bringing them into the ALB operational frequency range. Hence, the effort to include this effect into the mathematical model is justified.

The approach presented here is based on the method presented in [32]. Refering to Fig.4, the pipeline is considered as a one dimensional domain, and the magnitudes to be studied are the flow q_P and the pressure p_P along the longitudinal position x_P. For the analyzed domain, one dimensional continuity and Navier-Stokes equations can be applied, yielding the following system of equations:

$$\begin{aligned} \frac{\partial p_P}{\partial t} + \frac{\rho c_0^2}{A_P}\frac{\partial q_P}{\partial x_P} &= \frac{\rho c_0^2}{A_P} S_q \\ \frac{\partial q_P}{\partial t} + \frac{A_P}{\rho}\frac{\partial p_P}{\partial x_P} &= \frac{F_{ext}}{\rho} \end{aligned} \tag{4}$$

In Eqn. (4), the continuity equation is stated considering the variation of the flow rate q_P along the pipeline due to compressibility effects and the presence of sources or sinks S_q. The Navier-Stokes equation accounts for the variation of the linear momentum of the flow due to the pressure gradient and the externally applied forces F_{ext}, such as the ones arising from

viscous effects. The boundary conditions are:

$$\begin{aligned} q_P(x_P = 0, t) &= q_V \\ p_P(x_P = L_P, t) &= p_{inj} \end{aligned} \tag{5}$$

The boundary conditions stated in Eqn. (5) represent the servovalve flow q_V in the pipe entry point $x_P = 0$, and the pressure in the injection nozzle p_{inj}, located in the pipe exit $x_P = L_P$. The system of equations is then solved analytically using the separation of variables method [32]. This method entails obtaining the pipeline flow $q_P(x_P, t)$ as a superposition of modal flows $\gamma_{P_i}(t)$ corresponding to the acoustic normal modes $H_i(x_P)$, associated with the acoustic natural frequencies ω_{P_i}. Hence, one obtains:

$$\begin{aligned} q_P(x_P, t) &= \sum_{i=1}^{\infty} H_i(x_P)\,\gamma_{P_i}(t) \\ \omega_{P_i} &= \frac{(2i-1)\,\pi c_0}{2L_P} \\ H_i(x_P) &= sin\left(\frac{\omega_{P_i} x_P}{c_0}\right) \\ \ddot{\gamma}_{P_i} + c_P\dot{\gamma}_{P_i} + \omega_{P_i}^2\gamma_{P_i} &= \frac{2c_0\omega_{P_i}}{L_P} q_V - \frac{2A_P}{\rho L_P}\dot{p}_{inj}(-1)^{i+1} \end{aligned} \tag{6}$$

The evaluation of Eqn. (6) for $x_P = L_P$ and a finite number of modes provides the means for calculating the injected oil flow into the bearing clearance $q_P(x_P = L_P, t)$. Truncating the solution to a finite number of modes comes with the risk of obtaining a solution that violates mass conservation in the system. Hence, higher modes must be included in the solution, even though they do not contribute to the system dynamics in terms of resonance areas in the studied frequency range.

Related to the equivalent damping coefficient for the pipeline dynamic analysis c_P, it is assumed that the pipeline losses can be modeled using the Hagen-Pouiseuille equation. Hence, the damping coefficient is given by [32]:

$$c_P = \frac{8\mu}{\rho r_P^2} \tag{7}$$

3.3 Linking the Hydraulic System and the Oil Film Pressure Field

In order to include the effect of the injected oil flow over the oil film pressure field, the method outlined in [4, 14] is applied. The oil film pressure field $p(\hat{x}, \hat{z})$ is analyzed using a curvilinear reference frame $\hat{x}, \hat{y}, \hat{z}$ where the $\hat{x}$ coordinate is aligned in the circumferential direction, and the $\hat{z}$ coordinate is aligned in the axial direction, see Fig.5. Given that the injection nozzle has a diameter d_{inj} and length l_{inj}, it is assumed that the injection flow can be described as a Hagen-

Pouiseuille fully developed laminar flow. Hence, the injection velocity profile is given by [4, 14]:

$$v_{inj}(\hat{x},\hat{z},t) = \frac{1}{4\mu_{inj}}\left(\frac{p_{inj}(t) - p(\hat{x},\hat{z},t)}{l_{inj}}\right) g(\hat{x},\hat{z}) \tag{8}$$

Where the $g(\hat{x},\hat{z})$ function is defined as:

$$\begin{aligned} g(\hat{x},\hat{z}) &= \frac{d_{inj}^2}{4} - (\hat{x}-\hat{x}_{inj})^2 - (\hat{z}-\hat{z}_{inj})^2 \ , \ \textit{over the nozzle} \\ g(\hat{x},\hat{z}) &= 0 \ , \ \textit{over the pad surface} \end{aligned} \tag{9}$$

The integration of the velocity profile given in Eqn. (8) over the injection nozzle surface S_{inj} provides the injection flow. Such injection flow is equal to the pipeline flow modeled in the previous section:

$$q_P(x_P = L_P, t) = \int_{S_{inj}} v_{inj}(\hat{x},\hat{z},t)\, dS \tag{10}$$

To complete the link between the hydraulic system and the oil film pressure field, the injection velocity profile described in Eqn. (8) is implemented as a boundary condition for the oil film velocity field in the radial direction [4, 14]. Keeping the rest of the simplifying assumptions used for obtaining the Reynolds equation, the following is obtained:

$$\frac{\partial}{\partial\hat{x}}\left(\frac{h^3}{\mu}\frac{\partial p}{\partial\hat{x}}\right) + \frac{\partial}{\partial\hat{z}}\left(\frac{h^3}{\mu}\frac{\partial p}{\partial\hat{z}}\right) = 6\Omega R\frac{\partial h}{\partial\hat{x}} + 12\frac{\partial h}{\partial t} + 12v_{inj} \tag{11}$$

Introducing the definition of v_{inj} given by Eqn. (8), the modified Reynolds equation can be stated as:

$$\frac{\partial}{\partial\hat{x}}\left(\frac{h^3}{\mu}\frac{\partial p}{\partial\hat{x}}\right) + \frac{\partial}{\partial\hat{z}}\left(\frac{h^3}{\mu}\frac{\partial p}{\partial\hat{z}}\right) = 6\Omega R\frac{\partial h}{\partial\hat{x}} + 12\frac{\partial h}{\partial t} + 3g\frac{(p - p_{inj})}{\mu_{inj} l_{inj}} \tag{12}$$

3.4 Linearization of the Constitutive Equations: ALB Calibration Function

In summary, if only the first pipeline modal flow is included, the ALB hydraulic system is modeled by:

$$
\begin{aligned}
q_{V_A} &= q_V^* + q_{x_V} - K_{pq}\left(p_{inj_A} - p_{inj_B}\right) \\
q_{V_B} &= q_V^* - q_{x_V} + K_{pq}\left(p_{inj_A} - p_{inj_B}\right) \\
\ddot{q}_{x_V} &+ 2\xi_V \omega_V \dot{q}_{x_V} + \omega_V^2 q_{x_V} = \omega_V^2 R_V u_V \\
\ddot{q}_{P_A} &+ c_P \dot{q}_{P_A} + \omega_P^2 q_{P_A} = \frac{2c_0\omega_P}{L_P} q_{V_A} - \frac{2A_P}{\rho L_P}\dot{p}_{inj_A} \\
\ddot{q}_{P_B} &+ c_P \dot{q}_{P_B} + \omega_P^2 q_{P_B} = \frac{2c_0\omega_P}{L_P} q_{V_B} - \frac{2A_P}{\rho L_P}\dot{p}_{inj_B}
\end{aligned}
\tag{13}
$$

And for the oil film pressure field, the governing equations are:

$$
\begin{aligned}
q_{P_A} &= \int_{S_{inj}} \frac{1}{4\mu_{inj}} \left(\frac{p_{inj_A} - p_A}{l_{inj}}\right) gdS \\
q_{P_B} &= \int_{S_{inj}} \frac{1}{4\mu_{inj}} \left(\frac{p_{inj_B} - p_B}{l_{inj}}\right) gdS \\
\frac{\partial}{\partial \hat{x}}&\left(\frac{h^3}{12\mu}\frac{\partial p_A}{\partial \hat{x}}\right) + \frac{\partial}{\partial \hat{z}}\left(\frac{h^3}{12\mu}\frac{\partial p_A}{\partial \hat{z}}\right) = \\
&\qquad \frac{\Omega R}{2}\frac{\partial h}{\partial \hat{x}} + \frac{\partial h}{\partial t} + g\frac{(p_A - p_{inj_A})}{4\mu_{inj} l_{inj}} \\
\frac{\partial}{\partial \hat{x}}&\left(\frac{h^3}{12\mu}\frac{\partial p_B}{\partial \hat{x}}\right) + \frac{\partial}{\partial \hat{z}}\left(\frac{h^3}{12\mu}\frac{\partial p_B}{\partial \hat{z}}\right) = \\
&\qquad \frac{\Omega R}{2}\frac{\partial h}{\partial \hat{x}} + \frac{\partial h}{\partial t} + g\frac{(p_B - p_{inj_B})}{4\mu_{inj} l_{inj}}
\end{aligned}
\tag{14}
$$

In Eqn. (13,14), the index A and B denotes the variables related to the bottom and top pad respectively. It can be observed that a positive value of the servovalve control signal u_V provides pressurized flow towards pad A, whereas a negative value redirects it towards pad B. The pipeline dynamics have been truncated to the first modal flow to ease the mathematical presentation of the coupled model, although for the actual calculations a higher number of modes is considered.

Applying FEM [16, 22, 23] to Eqn. (14) yields the discretized set of equations:

$$
\begin{aligned}
&\left[\mathbf{A}\left(\mathbf{x}_r, \mathbf{b}\right)\right]\left\{\mathbf{p}\right\} + \left[\mathbf{W}\right]\left\{\mathbf{p}_{inj}\right\} = \left\{\mathbf{r}\left(\mathbf{x}_r, \mathbf{b}, \dot{\mathbf{x}}_r, \dot{\mathbf{b}}\right)\right\} \\
&\left[\mathbf{W}\right]^T\left\{\mathbf{p}\right\} + \left[\mathbf{Q}\right]\left\{\mathbf{p}_{inj}\right\} = \left\{\mathbf{q}_P\right\}
\end{aligned}
\tag{15}
$$

In Eqn. (15), $\mathbf{p}_{inj} = \{p_{injA}, p_{injB}\}^T$ and $\mathbf{q}_P = \{q_{P_A}, q_{P_B}\}^T$. The matrices $\mathbf{W}$ and $\mathbf{Q}$ correspond to the FEM discretization of the integral that defines the Hagen-Pouiseuille flow in the injection nozzle, see Eqn. (10). It can be seen that the system

matrix $\mathbf{A}$ and the source term $\mathbf{r}$ related to the Reynolds equation solution are a function of the rotor position $\mathbf{x}_r$, and the pad displacements reduced to the modal coordinates $\mathbf{b}$, that define the oil film thickness function h. Considering a rigid rotor, and arranging the pad mode shapes vectors in a modal matrix $\mathbf{V}$, their dynamics can be modeled by [16, 22, 23]:

$$\begin{aligned} &[\mathbf{M}_r]\{\ddot{\mathbf{x}}_r\} = \{\mathbf{f}_r(\mathbf{p})\} + \{\mathbf{f}_{ext}\} \\ &[\mathbf{V}]^T[\mathbf{M}_b][\mathbf{V}]\ \{\ddot{\mathbf{b}}\} + [\mathbf{V}]^T[\mathbf{K}_b][\mathbf{V}]\ \{\mathbf{b}\} = [\mathbf{V}]^T\{\mathbf{f}_b(\mathbf{p})\} \end{aligned} \tag{16}$$

The coupled solution of Eqn. (13,15,16) defines the behavior of the ALB system. This non-linear system of equations can be integrated in time domain to determine the forces over the rotor $\mathbf{f}_r(\mathbf{p})$, as a function of the servovalve input signal u_V. Hence, it becomes possible to predict the ALB active forces, at the expense of considerable calculation time, due to the small time steps necessary to ensure accuracy in the numerical integration procedure.

Alternatively, by linearizing the system of equations given by Eqn. (13,15,16) it becomes feasible to perform a harmonic analysis instead. As a result, the ALB calibration function is directly obtained in the frequency domain, with a significant reduction of the calculation time. The linearization of the system is not only desirable from the point of view of the numerical implementation. The usage of the ALB as calibrated shaker for parameter identification requires that system perturbations are kept small, hence the linearized approach is also justified considering the experimental implementation of the identification procedure.

The modeling of the hydraulic system, Eqn. (13), corresponds to a lumped parameter approach, hence its governing equations are already of linear nature. Consequently, the main effort has to be focused on obtaining a linearized form of Eqn. (15,16). The method is based on the one presented in [16, 22, 23], with the modifications necessary for the application at hand. The system of non-linear equations can be rewritten as:

$$\begin{aligned} \Pi_1 &:= [\mathbf{A}(\mathbf{x}_r, \mathbf{b})]\{\mathbf{p}\} + [\mathbf{W}]\{\mathbf{p}_{inj}\} - \{\mathbf{r}(\mathbf{x}_r, \mathbf{b}, \dot{\mathbf{x}}_r, \dot{\mathbf{b}})\} \\ \Pi_2 &:= [\mathbf{W}]^T\{\mathbf{p}\} + [\mathbf{Q}]\{\mathbf{p}_{inj}\} - \{\mathbf{q}_P\} \\ \Pi_3 &:= [\mathbf{M}_r]\{\ddot{\mathbf{x}}_r\} - \{\mathbf{f}_r(\mathbf{p})\} - \{\mathbf{f}_{ext}\} \\ \Pi_4 &:= [\mathbf{V}]^T[\mathbf{M}_b][\mathbf{V}]\ \{\ddot{\mathbf{b}}\} + [\mathbf{V}]^T[\mathbf{K}_b][\mathbf{V}]\ \{\mathbf{b}\} - [\mathbf{V}]^T\{\mathbf{f}_b(\mathbf{p})\} \end{aligned} \tag{17}$$

Let $\mathbf{s}$ be the state of the system defined by its variables $\mathbf{s} = \{\mathbf{p}, \mathbf{p}_{inj}, \mathbf{b}, \mathbf{x}_r, \mathbf{q}_P, \mathbf{q}_V, q_{x_V}\}^T$. A first order Taylor expansion of the governing equations Π_i yields:

$$\begin{aligned} &\Pi_i(\mathbf{s}) \approx \Pi_i(\mathbf{s}^*) + \mathbf{J}_{\Pi i}(\mathbf{s} - \mathbf{s}^*) \\ &\mathbf{J}_{\Pi i} = \left[\frac{\partial \Pi_i}{\partial \mathbf{p}}\ \frac{\partial \Pi_i}{\partial \mathbf{p}_{inj}}\ \frac{\partial \Pi_i}{\partial \mathbf{b}}\ \frac{\partial \Pi_i}{\partial \mathbf{x}_r}\ \frac{\partial \Pi_i}{\partial \mathbf{q}_P}\ \frac{\partial \Pi_i}{\partial \mathbf{q}_V}\ \frac{\partial \Pi_i}{\partial q_{x_V}}\right] \end{aligned} \tag{18}$$

Where $\mathbf{s}^*$ is the state corresponding to the static equilibrium of the system, and $\mathbf{J}_{\Pi i}$ is the jacobian of each one of the Π_i functions. For any state $\mathbf{s}$ of the system, Eqn. (15,16) must hold. This condition is equivalent to keep $\Pi_i = 0$ for any state. Hence, Eqn. (18) reduces to:

$$\mathbf{J}_{\Pi i}(\mathbf{s}-\mathbf{s}^*) = \mathbf{J}_{\Pi i}\delta\mathbf{s} = \mathbf{0} \tag{19}$$

Eqn. (19) provides the formulation for obtaining an equivalent linearized system. The rotor is fixed in the experimental setup for obtaining the calibration function, yielding $\delta\mathbf{x}_r = 0$. Consequently, the rotor degrees of freedom are omitted from the linearized response of the system $\delta\mathbf{s}$, and the linearized system is defined as follows:

$$[\mathbf{A}^*]\{\delta\mathbf{p}\} + [\mathbf{W}]\{\delta\mathbf{p}_{inj}\} + [\mathbf{B}]\{\delta\mathbf{b}\} + [\mathbf{C}]\{\delta\dot{\mathbf{b}}\} = \mathbf{0} \tag{20}$$

$$[\mathbf{W}]^T\{\delta\mathbf{p}\} + [\mathbf{Q}]\{\delta\mathbf{p}_{inj}\} - \{\delta\mathbf{q}_P\} = \mathbf{0} \tag{21}$$

$$[\mathbf{V}]^T[\mathbf{M}_b][\mathbf{V}]\ \{\delta\ddot{\mathbf{b}}\} + [\mathbf{V}]^T[\mathbf{K}_b][\mathbf{V}]\ \{\delta\mathbf{b}\} - \{\mathbf{E}\} = \mathbf{0} \tag{22}$$

$$\delta q_{V_A} - \delta q_{x_V} + K_{pq}(\delta p_{inj_A} - \delta p_{inj_B}) = 0 \tag{23}$$

$$\delta q_{V_B} + \delta q_{x_V} - K_{pq}(\delta p_{inj_A} - \delta p_{inj_B}) = 0 \tag{24}$$

$$\delta\ddot{q}_{P_A} + c_P\delta\dot{q}_{P_A} + \omega_P^2\delta q_{P_A} - \frac{2c_0\omega_P}{L_P}\delta q_{V_A} + \frac{2A_P}{\rho L_P}\delta\dot{p}_{inj_A} = 0 \tag{25}$$

$$\delta\ddot{q}_{P_B} + c_P\delta\dot{q}_{P_B} + \omega_P^2\delta q_{P_B} - \frac{2c_0\omega_P}{L_P}\delta q_{V_B} + \frac{2A_P}{\rho L_P}\delta\dot{p}_{inj_B} = 0 \tag{26}$$

$$\delta\ddot{q}_{x_V} + 2\xi_V\omega_V\delta\dot{q}_{x_V} + \omega_V^2\delta q_{x_V} = \omega_V^2 R_V\delta u_V \tag{27}$$

In Eqn. (20), $\mathbf{A}^*$ is the system matrix associated to the Reynolds equation, calculated for the static equilibrium position. Following the procedure presented in [16, 22, 23], the **B**, **C** and **E** terms are calculated as:

$$\begin{aligned}
[\mathbf{B}] &= \frac{\partial[\mathbf{A}^*]}{\partial\mathbf{b}}\mathbf{p}^* - \frac{\partial\{\mathbf{r}\}}{\partial\mathbf{b}} \\
[\mathbf{C}] &= \frac{\partial[\mathbf{A}^*]}{\partial\dot{\mathbf{b}}}\mathbf{p}^* - \frac{\partial\{\mathbf{r}\}}{\partial\dot{\mathbf{b}}} \\
\{\mathbf{E}\} &= [\mathbf{V}]^T\{\frac{\partial\mathbf{f}_b}{\partial\mathbf{p}}\}^T\{\delta\mathbf{p}\}
\end{aligned} \tag{28}$$

In Eqn. (28) $\mathbf{p}^*$ is the pressure field for the static equilibrium position.

The initial non-linear system of equations has been reduced to a linearized system in which the interdependence between the different components of the ALB can be noted. The linearized oil film pressure field $\delta\mathbf{p}$ becomes a function of both the pad dynamics, represented by the terms containing the modal coordinates $\delta\mathbf{b}$, and the hydraulic system dynamics, represented by

the injection nozzles flow $\delta\mathbf{q}_P$, as it can be seen in Eqn. (20,21). Conversely, the pad dynamic response is a function of the linearized pressure field, see Eqn. (22). The hydraulic system is linked with the oil film domain through the injection flows term $\delta\mathbf{q}_P$ in Eqn. (21,25,26), which are a function of the servovalve flows $\delta\mathbf{q}_V$ in Eqn. (23,24), and of the pressure developed within the bearing clearance. The servovalve flow is a function of the control signal δu_V. Hence, the whole system dynamic response becomes a function of the electrical signal fed into the system.

The linearized system can be rearranged as follows:

$$\begin{aligned}
[\mathbf{M}_{ALB}]\{\delta\ddot{\mathbf{s}}\} + [\mathbf{D}_{ALB}]\{\delta\dot{\mathbf{s}}\} + [\mathbf{K}_{ALB}]\{\delta\mathbf{s}\} &= \{\delta\mathbf{f}_{ALB}\} \\
\{\delta\mathbf{s}\} &= \{\delta\mathbf{p}, \delta\mathbf{p}_{inj}, \delta\mathbf{b}, \delta\mathbf{q}_P, \delta\mathbf{q}_V, \delta q_{xv}\}^T \\
\{\delta\mathbf{f}_{ALB}\} &= \{\mathbf{0}, \mathbf{0}, \mathbf{0}, \mathbf{0}, \mathbf{0}, \delta u_V\}^T
\end{aligned} \tag{29}$$

Applying an excitation to the system defined by Eqn. (29) in the form of a harmonic input signal to the servovalve $\delta u_V = Ue^{i\omega t}$ and keeping the linearity assumption for the dynamic behavior of the coupled system, i.e. $\delta\mathbf{s} = \mathbf{S}e^{i\omega t}$, it is possible to solve for its stationary response. Hence, the complex valued amplitude $\mathbf{S}$ of the harmonic stationary response of the coupled system is obtained. The fact that the response amplitude is complex valued reflects the phase lag existing between the response of the servovalve, pipelines and pads, with respect to the servovalve control signal, due to the dynamics of these components.

Finally, the integration of the perturbed pressure field $\delta\mathbf{p}$ over the rotor surface yields the real and imaginary part of the active force F_{active}, as a function of the excitation frequency ω. Therefore, the frequency dependent ALB calibration function is obtained.

4 ALB calibration function: theoretical and experimental results

In this section, results regarding the prediction of the ALB calibration function are presented, obtained using the mathematical model defined in the previous section.

The bearing simulated here corresponds to the ALB test rig setup presented previously in Table 1. The finite element mesh used for the analysis is depicted in Fig.6. Only half of the pad is discretized to take advantage of the axial simmetry of the setup. The "solid" domain (pads) is discretized using tridimensional second order twenty node serendipity finite elements. The "fluid" domain (oil film) is discretized using bidimensional second order eight node quadrilateral elements, corresponding to one face of the "solid" serendipity elements. Mesh density is beyond the values required for convergence, according to the analysis presented in [23, 24].

The ALB static and thermal equilibrium state is determined using the Newton-Raphson method, as explained in [9, 17]. Then, the ALB calibration function is calculated by the method described in this article. The pad modal reduction scheme is implemented considering the three pad modes depicted in Fig. 7. Regarding pipeline dynamics a total of 50 acoustic modes are considered, in order to ensure mass conservation within acceptable tolerance in the hydraulic domain.

4.1 Validation of the Linearized Analysis

The first step is to validate the linearization procedure of the ALB governing equations. For doing this, the results delivered by the non-linear set of equations, see Eqn.(13,15,16), are considered as the benchmark. The procedure is to apply an excitation chirp function as the input signal for the servovalve u_V in the non-linear system, integrate in time the response of the system, and then use the time domain results to obtain the transfer function between input signal and resulting force over the rotor. The rotor is fixed, hence it does not present displacements for this analysis. Those results are compared against the ones obtained using the linearized form of the ALB governing equations, as exposed previously.

Fig. 8 depicts such comparison, for a certain set of operational parameters. The comparison has been performed for different set of parameters, yielding similar results. It can be seen that the results obtained using the two methods match almost identically, which validates the linearization approach presented before.

4.2 Effect of System Dynamics over the ALB Calibration Function

From the theoretical analysis presented before, it becomes clear that the coupling between the dynamics of the hydraulic system, the fluid film and bearing pads determine the overall behavior of the ALB calibration function. As a result of these dynamic effects, the active forces over the rotor will exhibit frequency dependency in both its magnitude and phase lag, relative to the servovalve control signal. The focus is set now to study the contribution of each specific element into the overall ALB dynamic response as an actuator.

The servovalve dynamic response is portrayed in Fig. 9. It can be seen that this component provides the first contribution regarding phase lag and frequency dependency of the ALB response with respect to the input signal u_V. Physically, the servovalve dynamics are related to the coupling between its fluid, solid and electromechanic domains. Their effect over the resulting flow is represented in a reduced manner using a second order differential equation, as shown before in Eqn. (3).

Once the oil is injected into the bearing clearance, the pressure field is perturbed and the resulting force over the rotor is modified. Such modification is also affected by the dynamic response of the pads to this excitation, as it was shown before in the theoretical analysis. The pad response can be decomposed in terms of its tilting motion, elastic deformations and pivot deflection, if a modal decomposition approach is established.

The effect of the pad dynamics over the ALB calibration function is analyzed in Fig.10. It can be seen that in general terms the calibration function follows the trend of the servovalve response regarding frequency dependency and phase lag effect, shown before in Fig. 9. The deviations from the servovalve response are related to the contribution from the pad and pivot dynamics. Regarding the effect of including different pad modes for the analysis, it can be seen that the results obtained for a rigid pad (tilting mode only), compliant pad (tilting and bending mode), and compliant pad with high pivot stiffness exhibit similar behavior between each other. The phase lag effect relative to the servovalve response obtained in such cases is negligible. A reduction of the pivot stiffness entails higher contribution from the pad dynamics into the overall response, specially in terms of a significant phase lag of the ALB active force with respect to the servovalve response.

Up to this point, no significant contribution from the pipeline dynamics can be observed in the system response. For obtaining the results presented so far, it has been assumed that the oil presents its nominal compressibility, i.e. there is not entrained

air within it. Any real hydraulic system presents a certain fraction of air entrained within the hydraulic fluid, which increases the effective compressibility of the fluid, therefore lowering the acoustic natural frequencies [25].

The influence of the air fraction within the oil over the ALB calibration function is portrayed in Fig.11. Only the pad rigid tilting motion is considered for the analysis, in order to isolate the contribution from the pipeline dynamics. It can be seen that an increase of the air percentage in the fluid brings the pipelines acoustic dynamics into the frequency range of application for the ALB, with the consequent modification of the injected flow and the resulting active forces.

4.3 Effect of Bearing Operational Conditions

The modification of the operational conditions of the bearing, namely rotor eccentricity and rotational speed, entails a modification of the ALB calibration function. Two effects come into play in such case. Firstly, when the hydrodynamic pressure is increased, due to higher eccentricity or rotational speed, a reduction of the injected oil flow is obtained. Secondly, a modification of rotor eccentricity or rotational speed entails that the oil film equivalent stiffness and damping are modified, with the consequent alteration of the pad dynamic response. Considering the theoretical model presented before, both of these effects will influence the ALB calibration function.

Fig.12 illustrates the influence of the bearing operational conditions over the calibration function. Only the tilting mode was included for the analysis, and the dynamics from the pipelines do not affect the results in the analyzed frequency range, since the acoustic natural frequencies lie outside the analyzed frequency range. It can be seen that for operational conditions where the hydrodynamic pressure is increased (higher eccentricity and rotational speed) a reduction of the magnitude of the active forces is obtained, while no significant change in the phase response is observed. These results are related to the change of pad dynamic response and injected flow, as stated before.

For this analysis, the pivot deformation effect was not included. It is known that the stiffness of the pivot is a function of the applied load over the pad [34], which is dependent of the hydrodynamic pressure. Consequently, when modifying the rotor eccentricity and rotational speed, the pad pivot mode response will be modified, due to the change in its equivalent stiffness, with the consequences already depicted in Fig. 10.

5 ALB Acting as Calibrated Shaker: Experimental Results

Up to this point, this study has proved by theoretical means the feasibility of using the ALB to generate active forces in a wide frequency range. Consequently, the ALB could be applied as a calibrated shaker to obtain a frequency response function and to perform modal parameter identification. This possibility is explored by experimental means in the current section.

A first step to this end is to obtain the ALB calibration function by experimental means. The ALB test rig can be setup as depicted in in Fig. 3, see configuration 1. Fig. 13 depicts the results obtained for a certain set of operational conditions. The obtained calibration function proves the feasibility of generating active forces in a wide frequency range using the ALB. It can be observed that one obtains measurable forces up to 200 Hz. Secondly, it becomes clear that the active forces present a phase lag relative to the servovalve response, due to the dynamics of the pipelines and bearing pads. Thirdly, the active

forces are modified depending on the bearing operational conditions.

To explore the use of the ALB as a calibrated shaker, the test rig is set up as shown in Fig. 3, see configuration 2. If a parameter identification procedure is performed using frequency domain analysis, the obtention of the frequency response function (FRF) of the system is the first step. For a one degree of freedom system, this function is defined as:

$$FRF(\omega) = \frac{Y(\omega)}{F(\omega)} \tag{30}$$

Considering the ALB test rig, $Y(\omega)$ corresponds to the vertical displacements of the rotor, and $F(\omega)$ to the force used to excite the system. When an electromagnetic shaker is used, this force is directly measured using a piezoelectric load cell. If the ALB is used as the excitation source, the measurable quantities are the vertical displacement of the rotor and the electric signal fed into the servovalve $U(\omega)$. Consequently, to obtain the system FRF the previously obtained calibration function $C(\omega)$ must be introduced in the following manner:

$$FRF(\omega) = \frac{Y(\omega)}{U(\omega)} \cdot \frac{U(\omega)}{F_{active}(\omega)} = \frac{Y(\omega)}{U(\omega)} \cdot C^{-1}(\omega) \tag{31}$$

Consequently, it is possible to obtain the system FRF using the electromagnetic shaker and following Eqn. (30), or the ALB if the relationship stated in Eqn. (31) is used. Fig. 14 and Fig. 15 depict the comparison between the two approaches. The results obtained using the shaker are considered as the benchmark. A chirp signal is used as input for the shaker and for the servovalve. The results are obtained for different supply pressures of the ALB hydraulic system and different amplitudes of the chirp signal fed into the servovalve.

In general, it can be seen that good agreement is obtained between the two methods, if care is taken in properly selecting the test parameters, i.e. amplitude of the input signal for the servovalve and supply pressure for the hydraulic system. If the values selected for these parameters entail a reduction of the pressurized flow reaching the pad injection nozzle (low signal amplitude and/or low supply pressure), then the amplitude of the active forces is reduced, with the consequent reduction of resulting rotor displacements and FRF coherence, as it can be seen in Fig. 14. Hence, the FRF obtained using the ALB deviates from the benchmark one.

If the pressurized flow is increased, by raising the supply pressure and/or amplitude of the input signal, the FRF coherence improves and the overall results resemble the benchmark ones in a better way, as it can be observed in Fig. 14 and Fig. 15. However, an upper limit for the increase in such parameters can be inferred from the results in Fig. 15. It can be seen that the system response is increased in the low frequency range, and decreased around the resonance area. This is equivalent to state that the equivalent stiffness and damping characteristics of the bearing have been modified due to the oil injection. Since the oil film flow pattern defines the dynamic properties of the bearing, care must be taken in keeping the perturbations due to the injection process to a minimum, to avoid modifying the original system dynamics when performing the parameter

identification procedure via ALB.

6 Conclusions and Future Aspects

This article has studied the feasibility of applying the tilting-pad journal bearing featuring the active lubrication (ALB) system as a calibrated actuator, in order to excite system dynamics in a wide frequency range. The investigation has been carried out by theoretical and experimental means. Theoretically, a mathematical multiphysics model has been formulated, which includes the dynamics of the tilting-pad bearing and associated hydraulic system. Such model has been reduced to a linearized form to obtain the calibration function of the controllable bearing as a function of the input signal frequency. Experimentally, the available ALB test rig has been used to characterize the calibration function of the studied bearing, as well as to gain insights about its application as a shaker for parameter identification purposes in turbomachinery.
The main conclusions arising from the study are listed as follows:

1. The theoretical model has enabled to determine the influence of the dynamics of the components of the ALB over the calibration function, i.e. the frequency dependent relationship between input signal and applied force over the rotor. It has been shown that the calibration function follows the trend of the servovalve response regarding frequency dependence and phase lag relative to the input signal, with deviations arising from the dynamics of pads and pipelines.
2. Regarding the effect of pad dynamics over the calibration function, the results show that the pivot stiffness effect and the resulting rigid body motion of the pad in the radial direction, can have a strong influence over the ALB calibration function, both in terms of magnitude and phase lag effect with respect to the input signal.
3. The pipeline dynamics can affect significantly the ALB calibration function, depending on the amount of air entrained in the oil flow. Higher percentage of entrained air entails higher resulting compressibility of the flow, with the resultant reduction of the acoustic natural frequencies of the pipeline. This entails an increase of the ALB active forces around the acoustic resonance, as well as an additional phase lag effect contribution to the global ALB calibration function.
4. The bearing operational conditions (i.e. hydrodynamic pressure developed in the oil film) modify the injected oil flow and the pad dynamic response, with the resulting modification of the ALB calibration function.
5. The experimental results regarding the ALB calibration function confirm the theoretical results, in terms of the ability of the system to generate forces in a wide frequency range, as well as regarding the phase lag effect existing between input signal and resulting force over the rotor.
6. The feasibility of using the active forces generated by the ALB to excite system dynamics has been proved experimentally, yielding good comparison with the benchmarking method. The usage of the ALB as a calibrated shaker demands for a careful selection of the hydraulic system parameters, i.e. supply pressure and amplitude of the input signal. The lower boundary for these parameters is dictated by the need of obtaining good coherence in the studied system FRF, entailing that a sufficient magnitude of the ALB active forces must be achieved. The upper boundary is determined by the need to keep the perturbation of the oil film flow pattern due to the injection process to a minimum, in order to keep the original system dynamics unaltered.

7. Future investigations will be focused on applying the ALB as a calibrated shaker in a experimental setup that resembles in a closer way an industrial application, i.e. a flexible rotor mounted on a tilting-pad journal bearing that features the active lubrication system. Furthermore, additional theoretical studies are underway to study the validity of the lumped parameter approach for modeling the hydraulic system, and the simplificatory assumptions to link the oil injection system with the bearing oil film.

References

[1] Glienicke, J., 1987. "Stabilitatsprobleme bei Lagerung schnellaufender Wellen - Berechnung, Konstruktion und Verhalten von Mehrflchen- und Kippsegmentlagern". *Technische Akademie Wuppertal, Germany*.

[2] Flack, R. D., and Zuck, C. J., 1988. "Experiments on the Stability of Two Flexible Rotor in Tilting Pad Journal Bearing". *Tribology Trans.,* **31**(2), pp. 251–257.

[3] Ulbrich, H., and Althaus, J., 1989. "Actuator Design for Rotor Control". *ASME Design Technical Conference: Proceedings of the 12th Bienial Conference on Mechanical Vibration and Noise*, pp. 17–22.

[4] Santos, I. F., 1994. "Design and Evaluation of Two Types of Active Tilting Pad Journal Bearings". In *The Active Control of Vibration*, C.R.Burrows and P.S.Keogh, eds. Mechanical Engineering Publications Limited, London, England, pp. 79–87.

[5] Santos, I., 1995. "On the Adjusting of the Dynamic Coefficients of Tilting-Pad Journal Bearings". *STLE Tribology Transactions,* **38**(3), pp. 700–706.

[6] Deckler, D., Veillette, R., Braun, M., and Choy, F., 2004. "Simulation and Control of an Active Tilting-Pad Journal Bearing". *STLE Tribology Transactions,* **47**(3), pp. 440–458.

[7] Wu, A., and De Queiroz, M., 2010. "A New Active Tilting-Pad Bearing: Non Linear Modeling and Feedback Control". *STLE Tribology Transactions,* **53**(5), pp. 755–763.

[8] Wu, A., Cai, Z., and De Queiroz, M., 2007. "Model-Based Control of Active Tilting Pad Bearings". *IEEE/ASME Transactions on Mechatronics,* **12**(6), December, pp. 689–695.

[9] Cerda, A., Bjerregaard Nielsen, B., and Santos, I. F., 2013. "Steady state characteristics of a tilting pad journal bearing with controllable lubrication: Comparison between theoretical and experimental results". *Tribology International,* **58**(1), pp. 85–97.

[10] Santos, I. F., 1996. "Theoretical and Experimental Identification on the Stiffness and Damping Coefficients of Active-Tilting Pad Journal Bearings". In *Identification in Engineering Systems*, M. Friswell and J. Mottershead, eds. The Cromwell Press Ltd., Swansea, Great Britain, pp. 325–334.

[11] Santos, I. F., and Scalabrin, A., 2003. "Control System Design for Active Lubrication with Theoretical and Experimental Examples". *Journal of Engineering for Gas Turbines and Power, ASME Trans.,* **125**, January, pp. 75–80.

[12] Santos, I. F., 2011. "Trends in Controllable Oil Film Bearings". *IUTAM Bookseries: Symposium on Emerging Trends in Rotor Dynamics,* **1011**, pp. 185–199.

[13] Santos, I. F., and Cerda, A., 2013. "Actively Lubricated Bearings Applied as Calibrated Shakers to Aid Parameter

Identification in Rotordynamics". *Proceedings of ASME Turbo Expo 2013*.

[14] Santos, I. F., and Russo, F., 1998. "Tilting-Pad Journal Bearings with Electronic Radial Oil Injection". *Journal of Tribology, ASME Trans.,* **120**(3), pp. 583–594.

[15] Santos, I. F., and Nicoletti, R., 1999. "THD Analysis in Tilting-Pad Journal Bearings using Multiple Orifice Hybrid Lubrication". *Journal of Tribology, ASME Trans.,* **121**, pp. 892–900.

[16] Haugaard, A. M., and Santos, I. F., 2010. "Multi-orifice Active Tilting-Pad Journal Bearings-Harnessing of Synergetic Coupling Effects". *Tribology International,* **43**(8), pp. 1374–1391.

[17] Cerda, A., and Santos, I. F., 2012. "Performance Improvement of Tilting-Pad Journal Bearings by means of Controllable Lubrication". *Mechanics & Industry,* **13**, pp. 17–32.

[18] Bjerregaard Nielsen, B., 2010. "Creation of a Mechatronic Tilting Pad Test Rig". Master Thesis, Technical University of Denmark.

[19] Santos, I. F., and Nicoletti, R., 2001. "Influence of Orifice Distribution on the Thermal and Static Properties of Hybridly Lubricated Bearings". *International Journal of Solids and Structures,* **38**, pp. 2069–2081.

[20] Cerda, A., Fillon, M., and Santos, I. F., 2012. "On the Simplifications for the Thermal Modeling of Tilting-Pad Journal Bearings under Thermoelastohydrodynamic Regime". *Proceedings of ASME Turbo Expo 2012*.

[21] Kim, J., Palazzolo, A., and Gadangi, R., 1995. "Dynamics Characteristics of TEHD Tilt Pad Journal Bearing Simulation including Multiple Mode Pad Flexibility". *ASME Journal of Vibration and Acoustics,* **117**(1), January, pp. 123–135.

[22] Haugaard, A. M., and Santos, I. F., 2010. "Stability of Multi Orifice Active Tilting-Pad Journal Bearings". *Tribology International,* **43**(9), pp. 1742–1750.

[23] Haugaard, A. M., 2010. "On Controllable Elastohydrodynamic Fluid Film Bearings". PhD Thesis, Technical University of Denmark.

[24] Cerda, A., 2013. "Mechatronics Applied to Fluid Film Bearings: Towards More Efficient Machinery". PhD Thesis, Technical University of Denmark.

[25] Merritt, H., 1967. *Hydraulic Control Systems*. Wiley and Sons, Inc.

[26] Santos, I. F., 1993. "Active Tilting Pad Bearings - Theory and Experiment". *VDI Fortschritt-Berichte, Reihe 11: Schwingungstechnik*(189).

[27] Edelmann, F., 1986. "High-Response Servovalves and their applications". *Hydraulik und Pneumatik*(30), pp. 1–6.

[28] Thayer, W., 1965. "Transfer Functions for MOOG Servovalves". *MOOG Technical Bulletin,* **103**, pp. 1–11.

[29] Watton, J., 1984. "The Generalized Response of Servovalve Controlled, Single Rod, Linear Actuators and the Influence of Transmission Line Dynamics". *ASME Journal of Dynamic Systems, Measurement and Control,* **106**, June, pp. 157–162.

[30] Watton, J., and Tadmori, M., 1988. "A comparison of techniques for the analysis of transmission line dynamics in electrohydraulic control systems". *Appl. Math. Modelling,* **12**, October, pp. 457–466.

[31] Matko, D., Geiger, G., and Gregoritza, W., 2000. "Pipeline Simulation Techniques". *Mathematics and Computers in Simulation,* **52**, pp. 211–230.

[32] Yang, L., Hals, J., and Moan, T., 2012. "Comparative Study of Bond Graph Models for Hydraulic Transmission Lines with Transient Flow Dynamics". *ASME Journal of Dynamic Systems, Measurement and Control,* **134**, May.

[33] Datta, B., Akella, S., and G.L., S., 1986. "Effect of Entrained Air on Dynamic Characteristics of Hydraulic Servosystem with Asymmetric Linear Motor". *Meccanica,* **21**, pp. 51–57.

[34] Kirk, R., and Reedy, S., 1988. "Evaluation of Pivot Stiffness for Typical Tilting-Pad Journal Bearing Designs". *ASME Journal of Vibration, Acoustics, Stress and Reliability in Design,* **110**, April, pp. 165–171.

LIST OF TABLE CAPTIONS

Table 1. Dimensions, oil properties and parameters of the test rig

LIST OF FIGURE CAPTIONS

Fig 1. Test rig for the tilting-pad bearing with active lubrication: the arrangement consists of a rigid rotor supported vertically by two tilting pads (1). The rotor is attached to a tilting frame (2), pivoted in one end. An hydraulic system consisting of a servovalve and pipelines (3) controls the pressurized oil flow towards the injection nozzle on each pad.

Fig 2. Tilting pads installed in the ALB test rig: the arrows show the position of the injection nozzles that render the bearing controllable

Fig 3. Schematics of the two configurations used for obtaining the experimental results presented in this study.

Fig 4. Schematics depicting the nomenclature used for analyzing the ALB hydraulic system.

Fig 5. Schematics depicting the nomenclature used for analyzing the ALB oil film pressure field.

Fig 6. Finite element mesh used for discretizing the oil film "fluid" domain (left) and pads "solid" domain (right)

Fig 7. Pad modes used for the modal reduction scheme: tilting motion (left), bending deformation (center), and pivot deformation (right)

Fig 8. Validation of the linearized analysis for obtaining the ALB calibration function $C(\omega)$: comparison between results obtained by time integration of the non-linear system, and by the harmonic analysis of the equivalent linearized system.

Fig 9. The servovalve response function, amplitude and phase lag of its response with respect to the input signal.

Fig 10. Effect of pad dynamics over the ALB calibration function, in amplitude and phase lag: comparison of results when including tilting mode (T), bending mode (B), and pivot deformation for a pivot stiffness of 10^9 $[N/m]$ (Piv1) and 10^8 $[N/m]$ (Piv2). Results obtained for rotor eccentricity 0.6 and rotational speed 3000 rpm. The servovalve response (SV) is given as reference.

Fig 11. Effect of pipeline dynamics over the ALB calibration function, in amplitude and phase lag: comparison of results for different fractions of air entrained within the oil flow. Results obtained for rotor eccentricity 0.6 and rotational speed 3000 rpm. The servovalve response (SV) is given as reference.

Fig 12.Effect of bearing operational conditions over the ALB calibration function, in amplitude and phase lag: comparison of results for different rotor eccentricities and rotational speeds. The servovalve response (SV) is given as reference.

Fig 13. Experimentally obtained ALB calibration function, in amplitude and phase lag. The servovalve spool response (SV) is given as reference.

Fig 14. Experimentally obtained FRF, comparison between results obtained using an electromagnetic shaker and the ALB as the excitation source, with two different amplitudes of the input chirp signal. The supply pressure for the ALB hydraulic system is 2 Mpa, rotor static loading is 400 N and rotational speed is 3000 rpm.

Fig 15. Experimentally obtained FRF, comparison between results obtained using an electromagnetic shaker and the ALB as the excitation source, with two different amplitudes of the input chirp signal. The supply pressure for the ALB hydraulic system is 8 Mpa, rotor static loading is 400 N and rotational speed is 3000 rpm.)

Table 1. Dimensions, oil properties and parameters of the test rig

Pad inner radius	49.923 *mm*
Journal radius	49.692 *mm*
Bearing axial length	100 *mm*
Assembly radial clearance	0.115 *mm*
Preload	0.5
Number of pads	2
Pad arc	69 *degrees*
Offset	0.5
Load Angle	on pad
Pad thickness	12 *mm*
Injection nozzle radius	3 *mm*
Injection pipeline length	1 *m*
Injection nozzle length	10 *mm*
Oil type	ISO VG22
Pad material	Brass
Pivot insert material	Steel
Pivot design	Rocker
Servovalve cut-off frequency ω_V	166 Hz
Servovalve leakage flow q_V^*	2e-6 m^3/s
Servovalve flow pressure coeff. K_{pq}	1.13e-12 $m^3/(sPa)$
Servovalve flow voltage coeff. R_V	33.4e-6 $m^3/(sV)$
Servovalve damping ratio ξ_V	0.6085

Journal of Vibration and Acoustics. Received November 19, 2013;
Accepted manuscript posted September 01, 2014. doi:10.1115/1.4028452

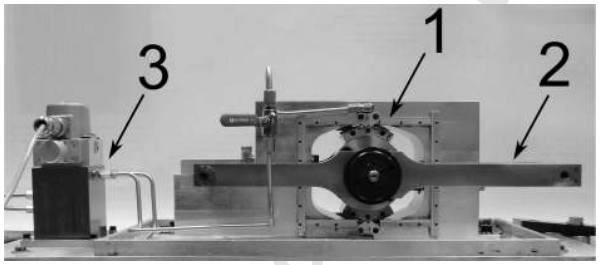

Fig. 1. Fig1.eps

Journal of Vibration and Acoustics. Received November 19, 2013;
Accepted manuscript posted September 01, 2014. doi:10.1115/1.4028452

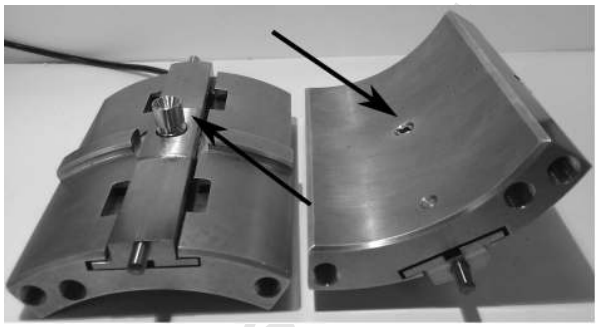

Fig. 2. Fig2.eps

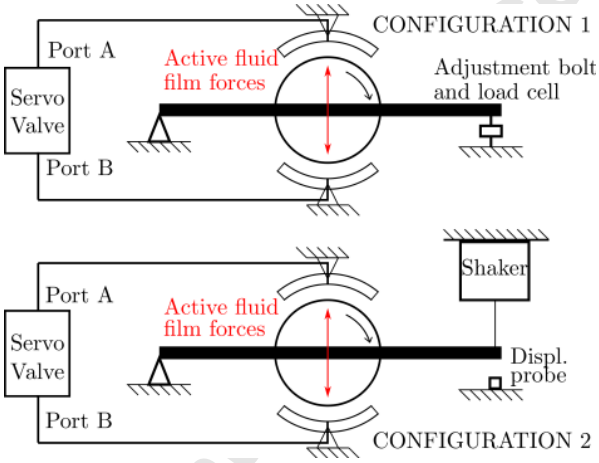

Fig. 3. Fig3.eps

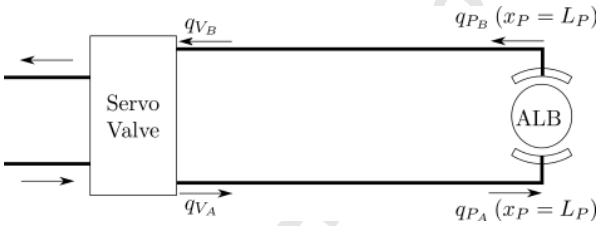

Fig. 4. Fig4.eps

Journal of Vibration and Acoustics. Received November 19, 2013;
Accepted manuscript posted September 01, 2014. doi:10.1115/1.4028452

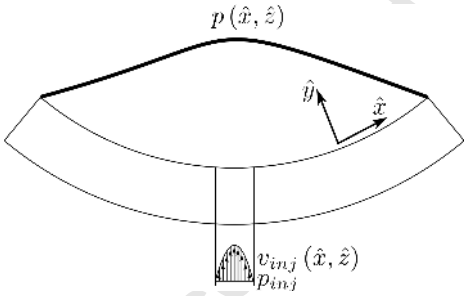

Fig. 5. Fig5.eps

Journal of Vibration and Acoustics. Received November 19, 2013;
Accepted manuscript posted September 01, 2014. doi:10.1115/1.4028452

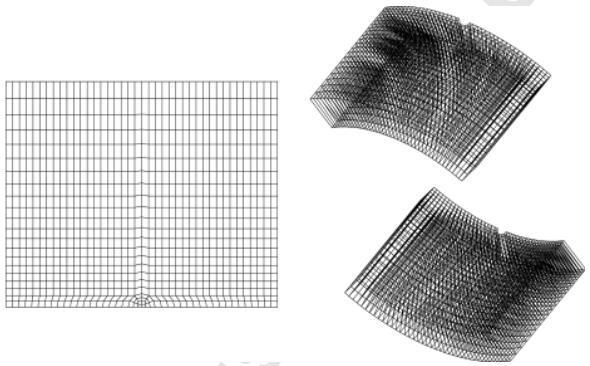

Fig. 6. Fig6.eps

Journal of Vibration and Acoustics. Received November 19, 2013;
Accepted manuscript posted September 01, 2014. doi:10.1115/1.4028452

Fig. 7. Fig7.eps

Journal of Vibration and Acoustics. Received November 19, 2013;
Accepted manuscript posted September 01, 2014. doi:10.1115/1.4028452

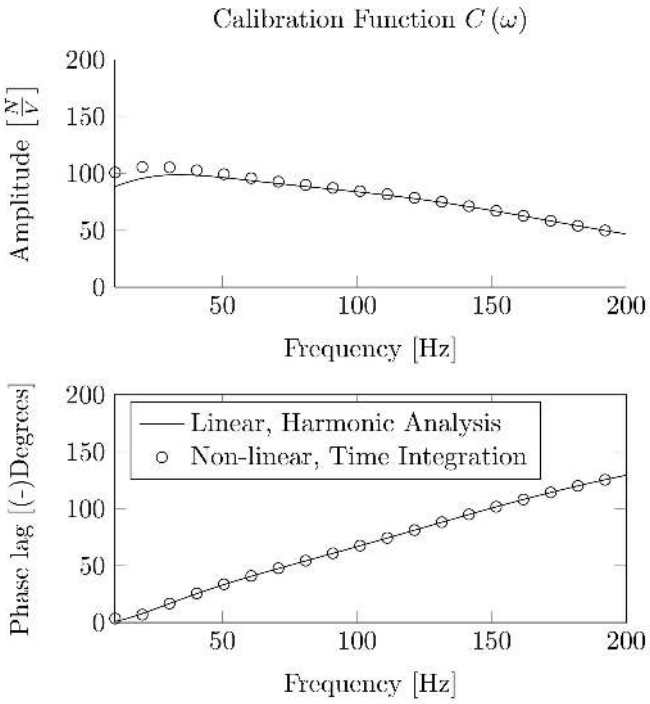

Fig. 8. Fig8.eps

Journal of Vibration and Acoustics. Received November 19, 2013;
Accepted manuscript posted September 01, 2014. doi:10.1115/1.4028452

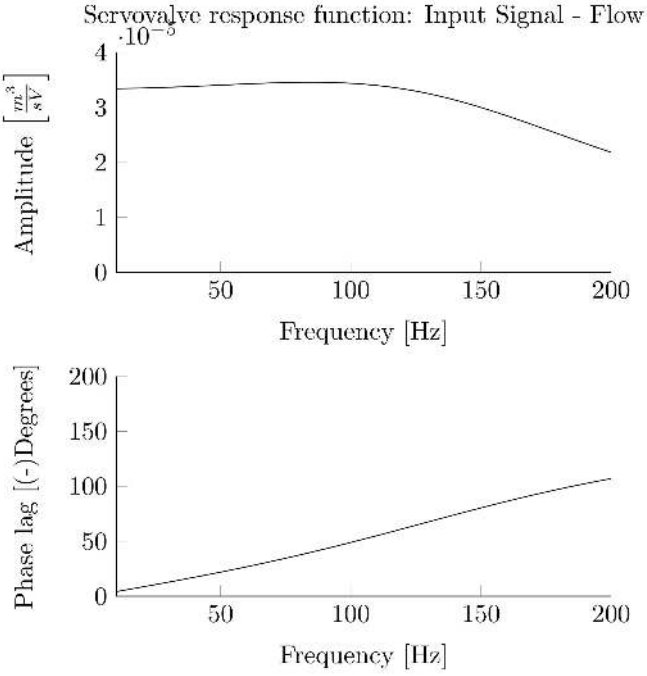

Fig. 9. Fig9.eps

Journal of Vibration and Acoustics. Received November 19, 2013;
Accepted manuscript posted September 01, 2014. doi:10.1115/1.4028452

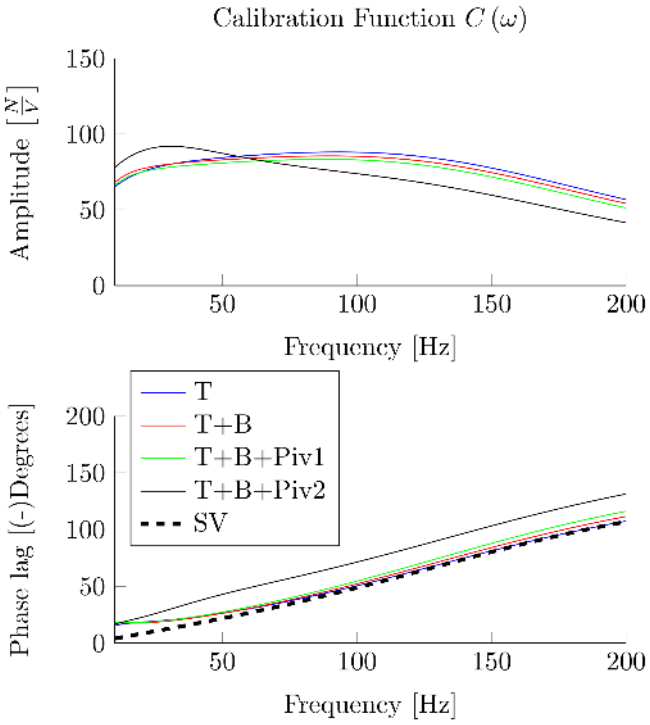

Fig. 10. Fig10.eps

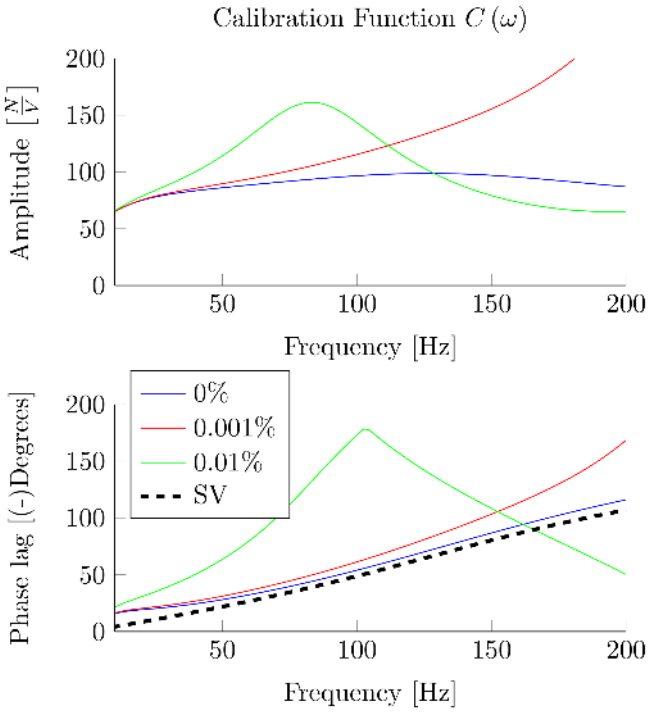

Fig. 11. Fig11.eps

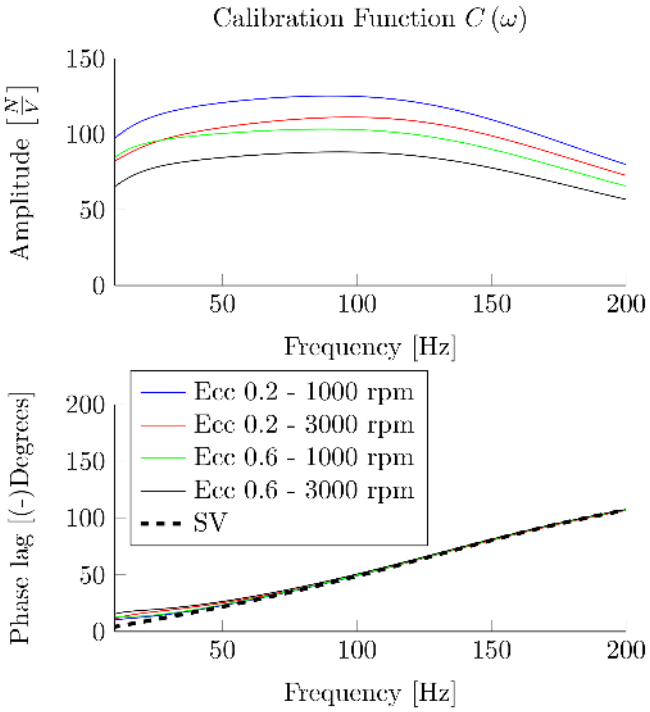

Fig. 12. Fig12.eps

Journal of Vibration and Acoustics. Received November 19, 2013;
Accepted manuscript posted September 01, 2014. doi:10.1115/1.4028452

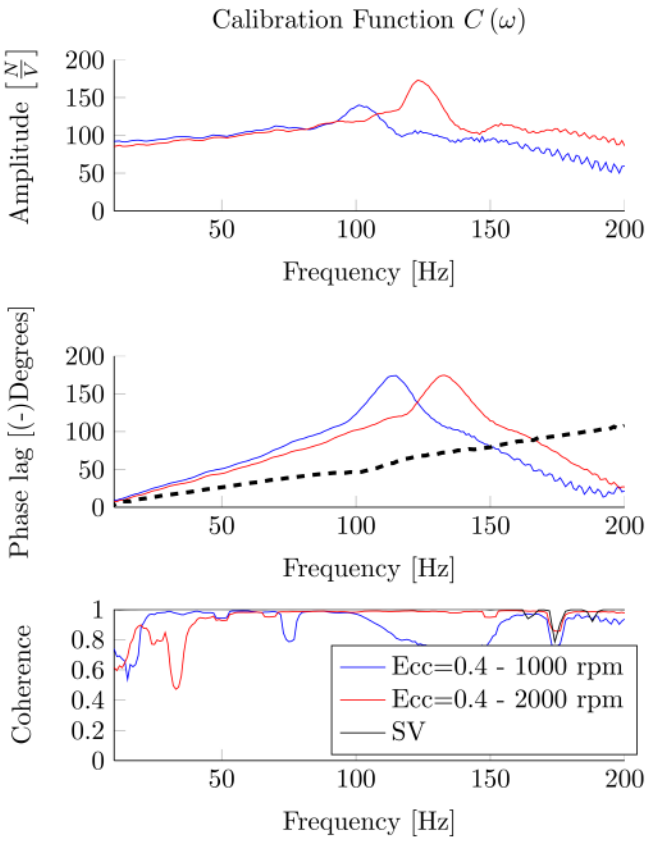

Fig. 13. Fig13.eps

Journal of Vibration and Acoustics. Received November 19, 2013;
Accepted manuscript posted September 01, 2014. doi:10.1115/1.4028452

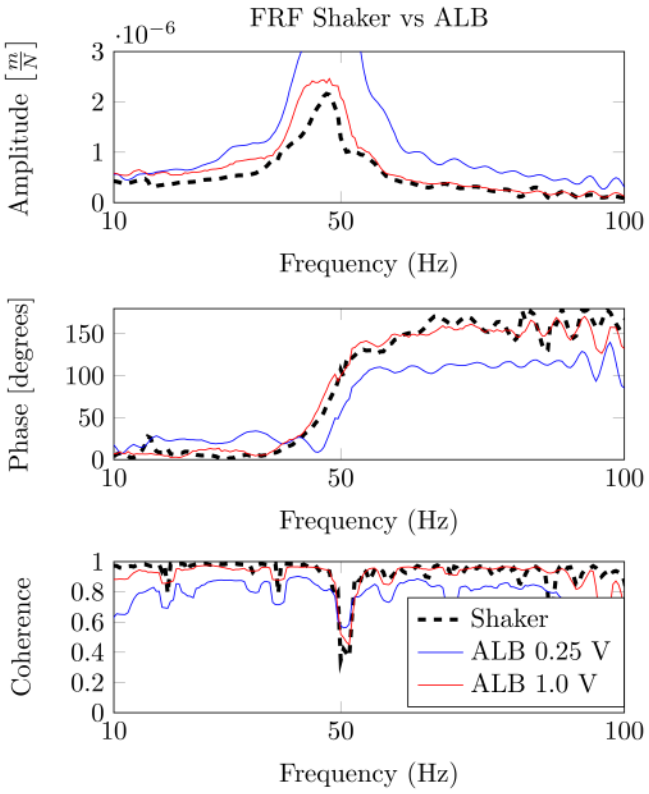

Fig. 14. Fig14.eps

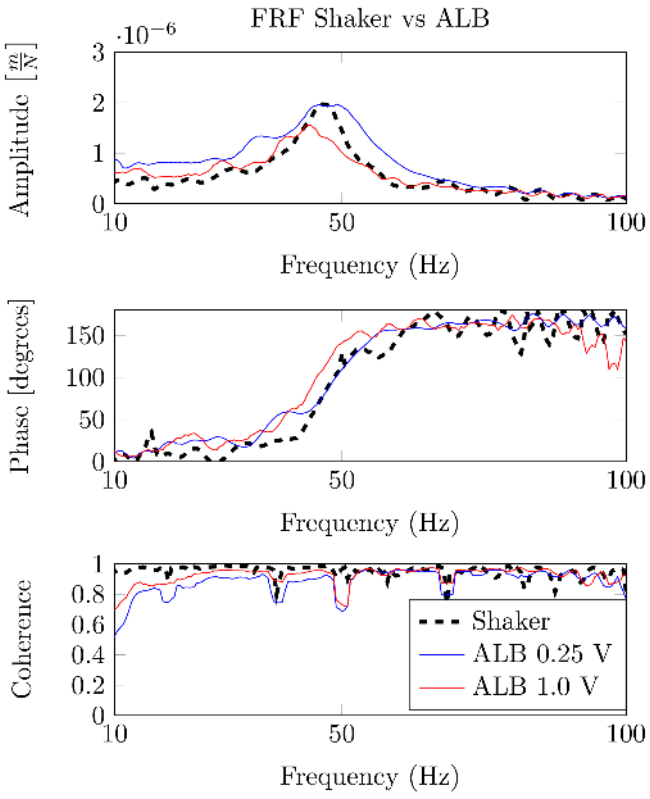

Fig. 15. Fig15.eps